Behaviors and energy source of Mycoplasma gallisepticum gliding

Behaviors and energy source of *Mycoplasma gallisepticum* gliding

Masaki Mizutani, Makoto Miyata

Citation	Journal of Bacteriology. 201(19); e00397-19
Issue Date	2019-09-06
Type	Journal Article
Textversion	author
Relation	The following article has been accepted by Journal of Bacteriology. After it is published, it will be found at https://doi.org/10.1128/JB.00397-19.
DOI	10.1103/PhysRevB.98.104419

Mizutani M, Miyata M. 2019. Behaviors and energy source of Mycoplasma gallisepticum gliding. *Journal of Bacteriol.* 201, e00397-19. https://doi.org/10.1128/JB.00397-19.

JB Accepted Manuscript Posted Online 15 July 2019
J. Bacteriol. doi:10.1128/JB.00397-19

To Journal of Bacteriology (Research article) (JB00317-19, ver3)

Behaviors and energy source of *Mycoplasma gallisepticum* gliding

Masaki Mizutani,[a] Makoto Miyata[a,b]#

[a]Graduate School of Science, Osaka City University, Sumiyoshi-ku, Osaka, Japan

[b]The OCU Advanced Research Institute for Natural Science and Technology (OCARINA), Osaka City University, Sumiyoshi-ku, Osaka, Japan

Running Title: *Mycoplasma* gliding behaviors

Address correspondence to Makoto Miyata, miyata@sci.osaka-cu.ac.jp

ABSTRACT

Mycoplasma gallisepticum, an avian-pathogenic bacterium, glides on host tissue surfaces by using a common motility system with *Mycoplasma pneumoniae*. In the present study, we observed and analyzed the gliding behaviors of *M. gallisepticum* in detail by using optical microscopes. *M. gallisepticum* glided at a speed of 0.27 ± 0.09 µm/s with directional changes relative to the cell axis of 0.6 ± 44.6 degrees/5 s without the rolling of the cell body. To examine the effects of viscosity on gliding, we analyzed the gliding behaviors under viscous environments. The gliding speed was constant in various concentrations of methylcellulose but was affected by Ficoll. To investigate the relationship between binding and gliding, we analyzed the inhibitory effects of sialyllactose on binding and gliding. The binding and gliding speed sigmoidally decreased with sialyllactose concentration, indicating the cooperative binding of the cell. To determine the direct energy source of gliding, we used a membrane-permeabilized ghost model. We permeabilized *M. gallisepticum* cells with Triton X-100 or Triton X-100 containing ATP and analyzed the gliding of permeabilized cells. The cells permeabilized with Triton X-100 did not show gliding; in contrast, the cells permeabilized with Triton X-100 containing ATP showed gliding at a speed of 0.014 ± 0.007 µm/s. These results indicate that the direct energy source for the gliding motility of *M. gallisepticum* is ATP.

IMPORTANCE

Mycoplasmas, the smallest bacteria, are parasitic and occasionally commensal. *Mycoplasma gallisepticum* is related to human pathogenic *Mycoplasmas*—*Mycoplasma pneumoniae* and *Mycoplasma genitalium*—which cause so-called ‘walking pneumonia’

and non-gonococcal urethritis, respectively. These *Mycoplasmas* trap sialylated oligosaccharides, which are common targets among influenza viruses, on host trachea or urinary tract surfaces and glide to enlarge the infected areas. Interestingly, this gliding motility is not related to other bacterial motilities or eukaryotic motilities. Here, we quantitatively analyze cell behaviors in gliding and clarify the direct energy source. The results provide clues for elucidating this unique motility mechanism.

INTRODUCTION

Members of the bacterial class *Mollicutes*, including the genus *Mycoplasma*, are parasitic, occasionally commensal, and characterized by small cells and genomes as well as the absence of a peptidoglycan layer (1, 2). More than ten *Mycoplasma* species, such as the fish pathogen *Mycoplasma mobile* (3-6) and the human pathogen *Mycoplasma pneumoniae* (6-8), have membrane protrusions and exhibit gliding motility in the direction of the membrane protrusion on solid surfaces, which enables *Mycoplasmas* to parasitize higher animals.

Interestingly, *Mycoplasma* gliding does not involve flagella or pili and is entirely unrelated to other bacterial motility systems and the conventional motor proteins that are common in eukaryotic motility systems (9, 10).

The gliding motilities of *Mycoplasmas* are classified into two systems; *M. mobile*-type and *M. pneumoniae*-type (5, 6). Although the appearance of gliding and the binding target, sialylated oligosaccharides (SOs) are common, the gliding mechanisms should be completely different, because they do not share any of the structures and the component proteins in the gliding machineries. It is remarkable that two gliding mechanisms were established independently in class *Mollicutes*, a rather small group of bacteria. *M.*

pneumoniae-type gliding has until now been studied mainly in *M. pneumoniae* and *Mycoplasma genitalium*. A structure outline of the gliding machinery has been suggested, including that for fifteen component proteins (6-8, 11). The gliding machinery, called the 'attachment organelle,' is composed of an internal core and adhesin complexes (12-14). The internal core is divided into three parts, the bowl complex, paired plates, and terminal button (3, 7, 13-15). It has been suggested that the bowl complex connects the internal core to the cell body and may be responsible for the generation or transmission of force (6, 16, 17). Furthermore, paired plates are the scaffold for formation and force transmission of the gliding machinery (6, 18-24). The terminal button is thought to tightly bind to the front side of the cell membrane (6, 23, 25-27). The adhesin complex is composed of P1 adhesin and P90 (28). P90 is encoded in tandem with P1 adhesin and is cleaved from another protein, P40, for maturation (29, 30). A recent study shows that the homolog of P40/P90 in *M. genitalium*, P110, has a binding pocket of SOs (31), which are binding targets for *Mycoplasma* infection and gliding. The mechanism of the gliding motility has been proposed as an 'inchworm model,' in which a cell catches SOs on solid surfaces through the adhesin complexes and is propelled by the repetitive extensions and retractions of the internal core (3, 6, 8). The gliding motility of *M. mobile* is driven by ATP using 'gliding ghost' which has a permeabilized membrane and can be reactivated by the addition of ATP (32-34). In contrast, the direct energy source for *M. pneumoniae*-type gliding motility is still unclear (6).

Mycoplasma gallisepticum is an avian pathogen that causes chronic respiratory disease in chickens and infectious sinusitis in turkeys. The cells transmit from breeder birds to their progeny *in ovo* (1, 35, 36). *M. gallisepticum* glides using the *M. pneumoniae*-type

motility system and has eight homologs of component proteins of gliding machinery in *M. pneumoniae* whose identities for amino acids range from 20% to 45% (36-39). The structure of the gliding machinery is similar to that in *M. pneumoniae* (37, 39). *M. gallisepticum* has a faster growth rate and more stable cell shape than *M. pneumoniae*, which is beneficial for the motility study (37).

In this study, we observe and analyze the gliding behaviors of *M. gallisepticum* in detail, and clarify the direct energy source of the gliding motility by modified gliding ghost experiments.

RESULTS

Gliding behaviors

The gliding motility of *M. gallisepticum* has been reported previously (37, 40), but the details have not yet been examined. Therefore, these details were examined in this study. *M. gallisepticum* cells were collected, suspended in phosphate-buffered saline (PBS) containing 10% non-heat-inactivated horse serum, and inserted into a tunnel chamber constructed by taping coverslips and precoated with non-heat-inactivated horse serum and bovine serum albumin. Then, the tunnel chamber was washed with PBS containing 20 mM glucose (PBS/G) and was observed by phase-contrast microscopy. We did not apply heat treatment to the serum, because the cells glided with much higher ratio with non-heated serum than heated one (37). The cells showed a flask shape (Fig. 1A) and glided in the direction of the tapered end, as previously reported (Fig. 1B; see Movie S1 in the supplemental material) (37). The complement in non-heated serum may be removed by the wash, alternatively it may not damage the gliding machinery. The proportions of gliding cells to all cells and the gliding speeds averaged for 60 s at 1 s

intervals were 62% ± 6% (n = 454) and 0.27 ± 0.09 μm/s (n = 231), respectively (Fig. 1B and C), which is consistent with those reported in the previous study (37). To analyze the gliding direction, we traced the angles between the cell axis and the following gliding direction for 60 s at 5 s intervals, as previously described (41). The averaged gliding direction relative to the cell axis was 0.6 ± 44.6 degrees/5 s (n = 231) (Fig. 1D), indicating that *M. gallisepticum* has no significant directional bias.

Possibility of rolling around the cell axis

A previous study shows that the adhesin complexes of *M. pneumoniae* exist around the membrane protrusion (8). *M. gallisepticum* may have a similar distribution because it uses similar gliding machinery to *M. pneumoniae* (36-39). The distribution of adhesin complexes suggests that cells may roll around the cell axis during gliding. To examine this possibility, we traced the movement of 40 nm colloidal gold labeled to a gliding cell. *M. gallisepticum* cells were biotinylated on the cell surface through amino groups, then mixed with 40 nm colloidal gold conjugated with streptavidin in the tunnel chamber and observed by dark-field microscopy. The cells labeled with colloidal gold glided at a similar speed to cells without colloidal gold (see Fig. S1 and Movie S2 in the supplemental material). All pairs of mass centers of cells and colloidal gold moved while maintaining a constant distance (n = 20) (Fig. 1E; see Fig. S1 in the supplemental material), showing that the cells glide without rolling of the cell body.

Gliding in viscous environments

A previous study shows that *M. mobile* gliding is drastically inhibited by viscous environments created using methylcellulose (MC) or Ficoll (41). To examine the effects of viscosity on *M. gallisepticum* gliding, we analyzed the gliding behaviors under viscous buffers including MC or Ficoll. MC is a long, linear, and slightly branched

polymer, and forms a gel-like three-dimensional network. Ficoll is a highly branched polymer which increases viscosity and does not form a network (42, 43). *M. gallisepticum* cells were suspended in PBS/G containing various concentrations of MC or Ficoll, inserted into the tunnel chamber, observed by phase-contrast microscopy, and analyzed for gliding speed and direction (Fig. 2A). The gliding speed did not significantly change with an increase in viscosity from 0.22 ± 0.06 μm/s (n = 50) at 0.66 mPa s to 0.19 ± 0.04 μm/s (n = 50) at 7.3 mPa s with 0% and 0.50% MC, respectively. However, the gliding speed did significantly decrease to 0.11 ± 0.04 μm/s (n = 50) at 4.6 mPa s with 15% Ficoll ($P<0.001$ by Student's *t*-test) (Fig. 2B and C). The averaged gliding direction relative to the cell axis did not change significantly with an increase in viscosity for all examined conditions. However, the standard deviations of gliding direction significantly decreased in Ficoll conditions ($P<0.001$ by F-test) from 27.4 degrees/5 s (n = 48) in 0% to 12.4 degrees/5 s (n = 50) in 15% Ficoll (Fig. 2B and C). These results indicate that the gliding motility of *M. gallisepticum* is affected by Ficoll but not MC.

Inhibition of binding and gliding by free sialyllactose

Previous studies show that *M. mobile* glides via dozens of working legs, the numbers of which can be reduced by the addition of free SOs (33, 44-46). To examine the relationship between binding and gliding, we added various concentrations of free 3′-*N*-acetylneuraminyllactose (3′-sialyllactose, SL), an SO, to gliding *M. gallisepticum* cells. The cell suspension was inserted into the tunnel chamber and observed by phase-contrast microscopy. After 60 s, the buffer was replaced by the buffers containing 0–0.5 mM SL. The gliding cells slowed down after the addition of free SL, and some of them detached from the glass surface (Fig. 3A and B). However, most of the cells which

were stopped by the addition of SL kept binding to glass at their front end of the membrane protrusion (see Fig. S2 in the supplemental material). The inhibition ratio for binding was calculated from the number of gliding cells at 40 s after the addition of SL to the number before the SL treatments (45). The ratio decreased with SL concentration from 88% ± 11% (n = 14) in 0 mM to 13% ± 11% (n = 21) in 0.5 mM SL (Fig. 3C). The gliding speed at 40 s after the addition of SL also decreased with SL concentration, from 0.17 ± 0.06 μm/s (n = 58) in 0 mM to 0.06 ± 0.04 μm/s (n = 54) in 0.5 mM SL (Fig. 3D). The Hill constant of binding was calculated as previously described (45) to be about 1.55 (see Fig. S3 in the supplemental material), indicating cooperativity in binding between cells and SL.

Gliding ghost experiment for specification of direct energy source

Previous studies show that the gliding motility of *M. mobile* is driven by ATP hydrolysis based on gliding ghost experiments. In these experiments, *M. mobile* cells were permeabilized with Triton X-100 and stopped for gliding. Gliding was then reactivated by the addition of ATP (32-34). In contrast, the reactivation of permeabilized cells of *M. pneumoniae*-type gliding *Mycoplasmas* has not been successful so far (6). At first, the same method was tried for *M. gallisepticum*, but about half of the cells permeabilized with Triton X-100 detached from the glass surfaces after the addition of ATP solution. Cells were permeabilized with Triton X-100 and ATP to efficiently observe the behaviors of permeabilized cells in the presence of ATP. This strategy was applied to *M. mobile* to confirm whether it was efficient. Cultured *M. mobile* cells were suspended in bufferA (10 mM HEPES pH 7.4, 100 mM NaCl, 2 mM $MgCl_2$, 1 mM EGTA, 1 mM DTT, 0.1% MC) containing 20 mM glucose and inserted into the tunnel chamber. We avoided to use phosphate buffer, because it inhibits phosphate release in ATPase activity

186 (32). Then, the cells were permeabilized with 0.013% Triton X-100 containing 1 mM
187 ATP + 0.01 mM ADP or 1 mM ADP. The cells permeabilized with Triton X-100
188 containing 1 mM ATP + 0.01 mM ADP glided at a similar speed to the intact cells. The
189 cells permeabilized with Triton X-100 containing 1 mM ADP stopped gliding when they
190 were permeabilized (see Movie S3 and S4 in the supplemental material). These results
191 indicate that this method works efficiently. This method was then applied to *M.*
192 *gallisepticum*. Cultured *M. gallisepticum* cells were suspended in bufferA containing
193 10% non-heat-inactivated horse serum, inserted into the tunnel chamber, washed by
194 bufferA containing 20 mM glucose, and observed by phase-contrast microscopy. Under
195 these conditions, the proportion of gliding cells to all cells and the averaged gliding
196 speed were 74% ± 3% (n = 2011) and 0.36 ± 0.06 μm/s (n = 220), respectively (see Fig.
197 S4 in the supplemental material). The buffer was then replaced by 0.007% Triton X-100
198 containing no ATP, 1 mM ATP + 0.01 mM ADP, or 1 mM ADP in bufferA. The cells
199 became round at 10–30 s from the addition of Triton solutions (Fig. 4A and B) causing
200 the gliding speeds to decrease (Fig. 4C; see Fig. S5 in the supplemental material). The
201 round cells showed three levels of cell-image density shifts; (i) the image density did
202 not decrease, (ii) the image density decreased to be about 75% of the intact cell, (iii) the
203 image density decreased to half of the intact cell (Fig 4D and E; see Fig. S5 in the
204 supplemental material). The cells which decreased to be about 75% of the cell-image
205 density showed slow gliding when they were permeabilized with Triton X-100
206 containing 1 mM ATP + 0.01 mM ADP (Fig. 4A and C; see Fig. S5 and Movie S5 in the
207 supplemental material). The cells permeabilized with Triton X-100 containing no ATP
208 or 1 mM ADP solution did not show gliding (n_{intact} = 3943 and 2604, respectively) (Fig.
209 4F). These results indicate that we succeeded in forming gliding ghosts of *M.*

gallisepticum. The occurrence ratio of gliding ghosts was calculated to be 0.41% from the numbers of gliding ghosts and intact cells before Triton treatment (n_{intact} = 11528 and n_{ghost} = 47). The gliding speed of ghosts in 1 mM ATP + 0.01 mM ADP was averaged for 150 s at 10-s intervals and found to be 0.014 ± 0.007 μm/s (Fig. 4G). The 62.9% of gliding ghosts continued to glide for 17 min of video recording. In the ATP hydrolysis cycle, the ATP state becomes the ADP or P_i state through the ADP + P_i state. Vanadate ion (V_i) with ADP can mimic the ADP + P_i state. V_i acts as a phosphate analog to form an ADP-V_i complex which occupies the catalytic site of ATPase and blocks the hydrolysis cycle (47, 48). The cells were permeabilized with Triton containing 1 mM ATP + 0.5 mM V_i to examine whether V_i affects the gliding of ghosts, (Fig. 4F). The gliding ghosts in ATP + V_i glided with 0.011 ± 0.010 μm/s (n = 9) at an occurrence ratio of ghost to all intact cells 0.37% (n_{intact} = 2439 and n_{ghost} = 9) (Fig. 4H and I), similar to the ghosts constructed by Triton X-100 containing 1 mM ATP + 0.01 mM ADP. However, only 33.3% of ghosts continued to glide for 17 min of video recording under ATP + V_i conditions, which is half of the ghosts constructed by Triton X-100 containing 1 mM ATP + 0.01 mM ADP (Fig. 4J), suggesting that V_i gradually stopped the gliding of ghosts. These results indicate that the gliding motility of *M. gallisepticum* is driven by ATP hydrolysis.

Damage to cell membranes by treatment with Triton X-100

Cells treated with 0.007% Triton X-100 became round and showed three levels of cell-image density shifts (Fig. 4D and E; see Fig. S5 in the supplemental material). Negative-staining electron microscopy was carried out to analyze the morphological changes and the cell-image density shifts observed under optical microscopy in detail. Intact cells showed a pear-shape with a membrane protrusion called a ‘bleb’ and

'infrableb,' as previously reported (Fig. 5A) (37, 49). Cells treated with Triton X-100 solution containing 1 mM ATP + 0.01 mM ADP showed a round cell shape (Fig. 5B), consistent with our observations by optical microscopy. Some of the cells had large or small holes on the cell membrane (Fig. 5C−E). These results indicate that the cells treated with Triton X-100 solution have a permeabilized membrane causing the loss of cytoplasm. We could not distinguish the permeabilized cells corresponding to those with 75% and half cell density of original cells which were observed in the optical microscopy (Fig. 4).

DISCUSSION

Gliding behaviors

In the present study, we observed and analyzed the gliding behaviors of *M. gallisepticum* by using optical microscopes. The gliding speed of *M. gallisepticum* measured in the present study was about 0.27 μm/s (Fig. 1C), which is comparable to the reported gliding speeds of *M. pneumoniae* and *M. genitalium*, about 0.64 μm/s and 0.15 μm/s, respectively (39). A previous study shows that *M. genitalium* has curved attachment organelles and a circular trajectory of gliding, but the deletion mutant of MG_217 protein shows straight attachment organelles and a straight trajectory, suggesting that the gliding direction is determined by the alignment of the attachment organelle (23). *M. gallisepticum* does not have a strong bend in attachment organelles (Fig. 5A) (37), and the average gliding direction was 0.6 ± 44.6 degrees/5 s (Fig. 1D), which is consistent with previous observations (23, 41). However, cells sometimes glided to the left or the right (Fig. 1B). In these cases, the cells bind to glass surfaces at the end of the membrane protrusion so that the thermal fluctuations and drag of the cell

body likely changes the gliding direction to left or right.

M. gallisepticum did not roll around the cell axis during gliding (Fig. 1E; see Fig. S1 in the supplemental material). Previous studies show that *M. mobile* does not roll even with adhesin complexes working as a 'leg' around the membrane protrusion (41, 50, 51). *M. gallisepticum* and *M. mobile* glide on the ciliated epithelial cells of birds and the gills of fresh-water fish in nature, respectively. The distribution of adhesin complexes may be an advantage for binding to host surfaces because these tissue surfaces are three-dimensionally aligned.

In this study, it was found that Ficoll has inhibitory effects on *M. gallisepticum* gliding but MC does not (Fig. 2). The reduction of gliding speed by Ficoll is unlikely caused by the increased friction applied to the cell body, because the force generated by friction is estimated as 2.3 fN even in the highest Ficoll concentration used here (52). Considering that the force generated by a single motor proteins ranges 2-7 pN and the force of *M. mobile* gliding ranges 27-113 pN, the 2.3 fN cannot reduce the gliding speed (46, 53-56). Perhaps, Ficoll interrupts the conformational changes of adhesion complex involved in the gliding mechanism, as suggested for *M. mobile* gliding (41). This assumption is consistent with the observation that MC does not reduce the gliding speed even if it increases the solution viscosity to the similar level to that by Ficoll.

Cooperativity in binding

Binding and gliding speed sigmoidally decreased by free SL (Fig. 3C and D), suggesting that the adhesin complex on the *M. gallisepticum* cells work cooperatively. Previous studies show that one adhesin complex of *M. pneumoniae* is composed of two heterodimers, one of each is assembled by one P1 adhesin molecule and one P90 molecule (28). The adhesin complex in *M. genitalium* is also composed of a dimer of

heterodimers constructed by P110 and P140, the homologs of P1 adhesin and P90, respectively (57). P110 has a binding site for SOs, so one adhesin complex binds two SOs (31). The adhesin complex of *M. gallisepticum* is assumed to have two binding sites for SOs because the components adhesin complex, CrmA and GapA have similarity with P110 and P140, respectively, in their amino acid sequences. This assumption is consistent with 1.55 of the Hill constant, a parameter presenting cooperativity (see Fig. S3 in the supplemental material). The Hill constant of binding between *M. pneumoniae* cells and sialic compounds ranges from 1.5 to 2.5 (45), comparable to 1.55 of the Hill constant for *M. gallisepticum*.

In 0.5 mM SL conditions, cells rotating around the end of the membrane protrusion were observed (see Fig. S2 in the supplemental material). A previous study shows that the ghosts of *M. mobile* exhibit directed rotational motility around the membrane protrusion driven by the linear motion of the legs (34). In contrast, rotary motion in *M. gallisepticum* seems to be driven by thermal fluctuation because it has no regularity of rotational direction (see Fig. S2 in the supplemental material), suggesting the possibility that adhesin complexes exist with high density at the end of the membrane protrusion.

Energy source

In the present study, we succeeded in forming the gliding ghosts of *M. gallisepticum* and clarified that the direct energy source of gliding is ATP (Fig. 4). In this method, we added 0.01 mM ADP to 0.007% Triton X-100 and 1 mM ATP solution because cells permeabilized with 0.007% Triton X-100 and 1 mM ATP solution easily detached from glass surfaces, and the addition of ADP reduced these detachments.

In a previous study, the gliding ghosts of *M. mobile* glided at similar speeds to intact cells, and 85% of ghosts showed gliding (32). However, the gliding speed of *M.*

306 *gallisepticum* ghosts was 4% of that of the intact cells, and 0.4% of the intact cells
307 became gliding ghosts (Fig. 4I and J). Kawamoto *et al*. showed in 2016 that the
308 translucent area surrounding the internal core in *M. pneumoniae* might be occupied by
309 less-diffusive materials and play a role in transmitting the movements of the paired
310 plates originating in the bowl complex to the adhesin complexes (8). The low
311 occurrence ratio of gliding ghosts in *M. gallisepticum* may be caused by the
312 permeabilization of cells resulting in the elution of less-diffusive materials. The cells
313 treated with Triton X-100 show three levels of cell-image density shifts (Fig. 4D and E).
314 The cells which decreased in the cell-image density to be 75% of the intact cells
315 probably have permeabilized cell membranes which retain most of the less-diffusive
316 materials.
317 In the gliding motility of *M. mobile*, complexes of MMOBs 1660 and 1670 in internal
318 jellyfish-like structures have been proposed to hydrolyze ATP molecules as a motor (5,
319 58). Therefore, which proteins work as a motor in the *M. pneumoniae*-type gliding
320 system need to be identified. Fifteen component proteins of the attachment organelles in
321 *M. pneumoniae* have been identified until now (6). One of these proteins has been
322 annotated as Lon, an ATP-dependent protease (6). This protein possibly works as a
323 motor for gliding.
324 Generally, respirable bacteria generate a proton gradient across the cell membrane in the
325 respiratory process. The proton gradient causes proton motive force which drives F-type
326 ATP synthase and bacterial flagella (59, 60). However, *Mycoplasmas* have no genes for
327 electron transport and synthesize ATP molecules by glycolysis (61). The membrane
328 potential of *M. gallisepticum* was −48 mV, much smaller than that of typical bacteria,
329 which is −150 mV (62-65). Therefore, ATP is more convenient for *Mycoplasmas* for the

energy source of gliding motilities rather than proton motive force.

MATERIALS AND METHODS

Cultivation. The *M. gallisepticum* S6 strain was grown in Aluotto medium at 37°C, as previously described (37).

Observations of gliding behaviors. The cells were cultured to reach an optical density at 595 nm of around 0.1. The cultured cells were collected by centrifugation at 12,000 × *g* for 10 min at room temperature (RT) and suspended in PBS consisting of 75 mM sodium phosphate (pH 7.3) and 68 mM NaCl. The cell suspension was centrifuged at 12,000 × *g* for 5 min at RT, suspended in PBS containing 10% non-heat-inactivated horse serum (Gibco; Thermo Fisher Scientific, Waltham, MA), poured through a 0.45-μm pore size filter and incubated for 15 min at RT. Then, the cell suspension was poured twice more and inserted into a tunnel chamber which was assembled by taping coverslips cleaned with saturated ethanolic KOH and precoated with 100% non-heat-inactivated horse serum for 60 min and 10 mg/ml bovine serum albumin (Sigma-Aldrich, St. Louis, MO) in PBS for 60 min at RT. The tunnel chamber was washed with PBS containing 20 mM glucose, incubated at 37°C on an inverted microscope (IX83; Olympus, Tokyo, Japan) equipped with a thermo plate (MATS-OTOR-MV; Tokai Hit, Shizuoka, Japan) and a lens heater (MATS-LH; Tokai Hit), observed by phase-contrast microscopy at 37°C and recorded with a charge-coupled device (CCD) camera (LRH2500XE-1; DigiMo, Tokyo, Japan). Video data were analyzed by ImageJ 1.43u (http://rsb.info.nih.gov/ij/), as previously described (37, 41).

To investigate the effect of viscosity on gliding, the cultured cells were washed with

PBS containing 10% non-heat-inactivated horse serum and 0.10%, 0.25%, and 0.50% MC (Methyl Cellulose #400; nacalai tesque, Kyoto, Japan) or 5%, 10%, and 15% Ficoll (M.W. 400,000; nacalai tesque, Kyoto, Japan), poured and incubated. Then, the cell suspension was poured and inserted into a cleaned and precoated tunnel chamber. The tunnel chamber was washed with various concentrations of viscous buffer containing 20 mM glucose, observed by phase-contrast microscopy at 37°C and recorded. The viscosities were measured using dynamic viscoelasticity measuring apparatus (Rheosol-G5000; UBM, Kyoto, Japan) at 37°C as follows: 0.66 mPa s for PBS/G, 2.5, 5.5, 7.3 mPa s for 0.10%, 0.25%, 0.50% MC, 2.3, 3.0, 4.6 mPa s for 5%, 10%, 15% Ficoll.

Cells on the tunnel chamber were treated with various concentrations of 3′-sialyllactose sodium salt (Nagara Science Co., Ltd, Tokyo, Japan) in PBS/G, observed by phase-contrast microscopy at 37°C and recorded to examine the binding features.

The cultured cells were collected, suspended in PBS containing 10 mM Sulfo-NHSLC-LC-Biotin (Thermo Fisher Scientific) and incubated for 15 min at RT to observe cell rolling. The cell suspension was centrifuged, suspended in PBS containing 10% non-heat-inactivated horse serum, poured, and incubated. Then, the cell suspension was poured and inserted into a cleaned and precoated tunnel chamber. The tunnel chamber was washed by PBS/G containing streptavidin conjugated 40 nm colloidal gold (Cytodiagnostics, Ontario, Canada), observed by dark-field microscopy using an upright microscope (BX50; Olympus) at 37°C and recorded by a CCD camera (WAT-120N; Watec Co. Ltd., Yamagata, Japan). Video data were analyzed by ImageJ 1.43u and IGOR Pro 6.33J (WaveMetrics, Portland, OR).

Gliding ghost

The cultured cells were collected and suspended in HEPES buffer (10 mM HEPES pH 7.4, 100 mM NaCl). The cell suspension was centrifuged, suspended in bufferA, poured, and incubated for 15 min at RT. Then, the cell suspension was poured and inserted into a cleaned and precoated tunnel chamber. The tunnel chamber was washed with bufferA containing 20 mM glucose, observed by phase-contrast microscopy at 37°C, and recorded. After 70 s, the buffer was replaced with 0.007% Triton X-100 (MP Biomedicals, Santa Ana, CA) containing 1 mM ATP and 0.01 mM ADP or 0 mM ATP or 1 mM ADP or 1 mM ATP and 0.5 mM Na_3VO_4. Video data were analyzed by ImageJ 1.43u.

Negative-staining electron microscopy. The cultured cells were collected, suspended in PBS containing 10% non-heat-inactivated horse serum, poured through a 0.45-µm pore size filter and incubated for 15 min at RT. Then, the cell suspension was placed on a carbon-coated grid and incubated for 10 min at RT. The grid was treated with 0.007% Triton X-100 containing 1 mM ATP and 0.01 mM ADP to permeabilize cells, incubated for 1 min at RT and fixed with 1% glutaraldehyde in bufferA for 1 min at RT. The fixed cells were washed with water, stained with 0.5% ammonium molybdate, and observed using a transmission electron microscope (JEM-1010; JEOL, Tokyo, Japan) at 80 kV equipped with a CCD camera (FastScan-F214 (T); TVIPS, Gauting, Germany).

ACKNOWLEDGMENTS

We thank Yuhei O Tahara at Osaka City University for technical assistance with negative-staining electron microscopy. This work was supported by a Grant-in-Aid for Scientific Research in the innovative area of ‘’Harmonized Supramolecular Motility Machinery and Its Diversity’ (Ministry of Education, Culture, Sports, Science, and

Technology KAKENHI; grant number 24117002), by a Grants-in-Aid for Scientific Research (A) (Ministry of Education, Culture, Sports, Science, and Technology KAKENHI; grant number 17H01544), and Jutenkenkyu from Osaka City University to M. Miyata. M. Mizutani is the recipient of a Research Fellowship of the Japan Society for the Promotion of Science (18J15362).

REFERENCES

1. Razin S, Yogev D, Naot Y. 1998. Molecular biology and pathogenicity of mycoplasmas. Microbiol Mol Biol Rev 62:1094-156.
2. Razin S, Hayflick L. 2010. Highlights of mycoplasma research--an historical perspective. Biologicals 38:183-90.
3. Miyata M. 2008. Centipede and inchworm models to explain *Mycoplasma* gliding. Trends Microbiol 16:6-12.
4. Miyata M. 2010. Unique centipede mechanism of *Mycoplasma* gliding. Annu Rev Microbiol 64:519-37.
5. Miyata M, Hamaguchi T. 2016. Prospects for the gliding mechanism of *Mycoplasma mobile*. Curr Opin Microbiol 29:15-21.
6. Miyata M, Hamaguchi T. 2016. Integrated information and prospects for gliding mechanism of the pathogenic bacterium *Mycoplasma pneumoniae*. Front Microbiol 7:960.
7. Nakane D, Kenri T, Matsuo L, Miyata M. 2015. Systematic structural analyses of attachment organelle in *Mycoplasma pneumoniae*. PLoS Pathog 11:e1005299.
8. Kawamoto A, Matsuo L, Kato T, Yamamoto H, Namba K, Miyata M. 2016. Periodicity in attachment organelle revealed by electron cryotomography suggests conformational changes in gliding mechanism of *Mycoplasma pneumoniae*. MBio 7:e00243-16.
9. Dandekar T, Huynen M, Regula JT, Ueberle B, Zimmermann CU, Andrade MA, Doerks T, Sanchez-Pulido L, Snel B, Suyama M, Yuan YP, Herrmann R, Bork P. 2000. Re-annotating the *Mycoplasma pneumoniae* genome sequence: adding value, function and reading frames. Nucleic Acids Res 28:3278-88.
10. Jaffe JD, Stange-Thomann N, Smith C, DeCaprio D, Fisher S, Butler J, Calvo S, Elkins T, FitzGerald MG, Hafez N, Kodira CD, Major J, Wang S, Wilkinson J,

Journal of Bacteriology

Nicol R, Nusbaum C, Birren B, Berg HC, Church GM. 2004. The complete genome and proteome of *Mycoplasma mobile*. Genome Res 14:1447-61.

11. Seybert A, Gonzalez-Gonzalez L, Scheffer MP, Lluch-Senar M, Mariscal AM, Querol E, Matthaeus F, Pinol J, Frangakis AS. 2018. Cryo-electron tomography analyses of terminal organelle mutants suggest the motility mechanism of *Mycoplasma genitalium*. Mol Microbiol 108:319-329.
12. Meng KE, Pfister RM. 1980. Intracellular structures of *Mycoplasma pneumoniae* revealed after membrane removal. J Bacteriol 144:390-9.
13. Henderson GP, Jensen GJ. 2006. Three-dimensional structure of *Mycoplasma pneumoniae*'s attachment organelle and a model for its role in gliding motility. Mol Microbiol 60:376-85.
14. Seybert A, Herrmann R, Frangakis AS. 2006. Structural analysis of *Mycoplasma pneumoniae* by cryo-electron tomography. J Struct Biol 156:342-54.
15. Hegermann J, Herrmann R, Mayer F. 2002. Cytoskeletal elements in the bacterium *Mycoplasma pneumoniae*. Naturwissenschaften 89:453-8.
16. Pich OQ, Burgos R, Ferrer-Navarro M, Querol E, Pinol J. 2006. *Mycoplasma genitalium mg200* and *mg386* genes are involved in gliding motility but not in cytadherence. Mol Microbiol 60:1509-19.
17. Jordan JL, Chang HY, Balish MF, Holt LS, Bose SR, Hasselbring BM, Waldo RH, 3rd, Krunkosky TM, Krause DC. 2007. Protein P200 is dispensable for *Mycoplasma pneumoniae* hemadsorption but not gliding motility or colonization of differentiated bronchial epithelium. Infect Immun 75:518-22.
18. Popham PL, Hahn TW, Krebes KA, Krause DC. 1997. Loss of HMW1 and HMW3 in noncytadhering mutants of *Mycoplasma pneumoniae* occurs post-translationally. Proc Natl Acad Sci U S A 94:13979-84.
19. Hahn TW, Willby MJ, Krause DC. 1998. HMW1 is required for cytadhesin P1 trafficking to the attachment organelle in *Mycoplasma pneumoniae*. J Bacteriol 180:1270-6.
20. Seto S, Miyata M. 2003. Attachment organelle formation represented by localization of cytadherence proteins and formation of the electron-dense core in wild-type and mutant strains of *Mycoplasma pneumoniae*. J Bacteriol 185:1082-91.
21. Kenri T, Seto S, Horino A, Sasaki Y, Sasaki T, Miyata M. 2004. Use of fluorescent-protein tagging to determine the subcellular localization of *Mycoplasma pneumoniae* proteins encoded by the cytadherence regulatory locus. J Bacteriol 186:6944-55.
22. Burgos R, Pich OQ, Querol E, Pinol J. 2007. Functional analysis of the

Mycoplasma genitalium MG312 protein reveals a specific requirement of the MG312 N-terminal domain for gliding motility. J Bacteriol 189:7014-23.

23. Burgos R, Pich OQ, Querol E, Pinol J. 2008. Deletion of the *Mycoplasma genitalium* MG_217 gene modifies cell gliding behaviour by altering terminal organelle curvature. Mol Microbiol 69:1029-40.
24. Bose SR, Balish MF, Krause DC. 2009. *Mycoplasma pneumoniae* cytoskeletal protein HMW2 and the architecture of the terminal organelle. J Bacteriol 191:6741-8.
25. Jordan JL, Berry KM, Balish MF, Krause DC. 2001. Stability and subcellular localization of cytadherence-associated protein P65 in *Mycoplasma pneumoniae*. J Bacteriol 183:7387-91.
26. Chang HY, Prince OA, Sheppard ES, Krause DC. 2011. Processing is required for a fully functional protein P30 in *Mycoplasma pneumoniae* gliding and cytadherence. J Bacteriol 193:5841-6.
27. Hasselbring BM, Sheppard ES, Krause DC. 2012. P65 truncation impacts P30 dynamics during *Mycoplasma pneumoniae* gliding. J Bacteriol 194:3000-7.
28. Nakane D, Adan-Kubo J, Kenri T, Miyata M. 2011. Isolation and characterization of P1 adhesin, a leg protein of the gliding bacterium *Mycoplasma pneumoniae*. J Bacteriol 193:715-22.
29. Layh-Schmitt G, Herrmann R. 1992. Localization and biochemical characterization of the ORF6 gene product of the *Mycoplasma pneumoniae* P1 operon. Infect Immun 60:2906-13.
30. Catrein I, Herrmann R, Bosserhoff A, Ruppert T. 2005. Experimental proof for a signal peptidase I like activity in *Mycoplasma pneumoniae*, but absence of a gene encoding a conserved bacterial type I SPase. FEBS J 272:2892-900.
31. Aparicio D, Torres-Puig S, Ratera M, Querol E, Pinol J, Pich OQ, Fita I. 2018. *Mycoplasma genitalium* adhesin P110 binds sialic-acid human receptors. Nat Commun 9:4471.
32. Uenoyama A, Miyata M. 2005. Gliding ghosts of *Mycoplasma mobile*. Proc Natl Acad Sci USA 102:12754-8.
33. Kinosita Y, Nakane D, Sugawa M, Masaike T, Mizutani K, Miyata M, Nishizaka T. 2014. Unitary step of gliding machinery in *Mycoplasma mobile*. Proc Natl Acad Sci USA 111:8601-6.
34. Kinosita Y, Miyata M, Nishizaka T. 2018. Linear motor driven-rotary motion of a membrane-permeabilized ghost in *Mycoplasma mobile*. Sci Rep 8:11513.
35. Levisohn S, Kleven SH. 2000. Avian mycoplasmosis (*Mycoplasma gallisepticum*).

Rev Sci Tech 19:425-42.

36. Indikova I, Vronka M, Szostak MP. 2014. First identification of proteins involved in motility of *Mycoplasma gallisepticum*. Vet Res 45:99.
37. Nakane D, Miyata M. 2009. Cytoskeletal asymmetrical dumbbell structure of a gliding mycoplasma, *Mycoplasma gallisepticum*, revealed by negative-staining electron microscopy. J Bacteriol 191:3256-64.
38. Indikova I, Much P, Stipkovits L, Siebert-Gulle K, Szostak MP, Rosengarten R, Citti C. 2013. Role of the GapA and CrmA cytadhesins of *Mycoplasma gallisepticum* in promoting virulence and host colonization. Infect Immun 81:1618-24.
39. Miyata M, Nakane D. 2013. Gliding mechanism of the *Mycoplasma pneumoniae* subgroup implications from studies on *Mycoplasma mobile*. in Molecular and Cell Biology of Mollicutes, eds G Browning and C Citti (Norfolk: Horizon Press):237–252.
40. Erdmann T. 1976. Untersuchungen zur morphologie, vermehrung und beweglichkeit von *Mycoplasma gallisepticum*. MD thesis Johannes Gutenberg Universita¨t, Mainz, Germany.
41. Morio H, Kasai T, Miyata M. 2016. Gliding direction of *Mycoplasma mobile*. J Bacteriol 198:283-90.
42. Magariyama Y, Kudo S. 2002. A mathematical explanation of an increase in bacterial swimming speed with viscosity in linear-polymer solutions. Biophys J 83:733-9.
43. Nakamura S, Adachi Y, Goto T, Magariyama Y. 2006. Improvement in motion efficiency of the spirochete *Brachyspira pilosicoli* in viscous environments. Biophys J 90:3019-26.
44. Nagai R, Miyata M. 2006. Gliding motility of *Mycoplasma mobile* can occur by repeated binding to *N*-acetylneuraminyllactose (sialyllactose) fixed on solid surfaces. J Bacteriol 188:6469-75.
45. Kasai T, Nakane D, Ishida H, Ando H, Kiso M, Miyata M. 2013. Role of binding in *Mycoplasma mobile* and *Mycoplasma pneumoniae* gliding analyzed through inhibition by synthesized sialylated compounds. J Bacteriol 195:429-35.
46. Mizutani M, Tulum I, Kinosita Y, Nishizaka T, Miyata M. 2018. Detailed analyses of stall force generation in *Mycoplasma mobile* gliding. Biophys J 114:1411-1419.
47. Shimizu T, Johnson KA. 1983. Presteady state kinetic analysis of vanadate-induced inhibition of the dynein ATPase. J Biol Chem 258:13833-40.
48. Burgess SA, Walker ML, Sakakibara H, Knight PJ, Oiwa K. 2003. Dynein structure

and power stroke. Nature 421:715-8.

49. Maniloff J, Morowitz HJ, Barrnett RJ. 1965. Ultrastructure and Ribosomes of *Mycoplasma gallisepticum*. J Bacteriol 90:193-204.
50. Miyata M, Uenoyama A. 2002. Movement on the cell surface of the gliding bacterium, *Mycoplasma mobile*, is limited to its head-like structure. FEMS Microbiol Lett 215:285-9.
51. Uenoyama A, Kusumoto A, Miyata M. 2004. Identification of a 349-kilodalton protein (Gli349) responsible for cytadherence and glass binding during gliding of *Mycoplasma mobile*. J Bacteriol 186:1537-45.
52. Rosengarten R, Kirchhoff H. 1988. Energetic aspects of the gliding motility of mycoplasmas. Current Microbiology 16:247-252.
53. Fujita K, Iwaki M, Iwane AH, Marcucci L, Yanagida T. 2012. Switching of myosin-V motion between the lever-arm swing and brownian search-and-catch. Nat Commun 3:956.
54. Kojima H, Muto E, Higuchi H, Yanagida T. 1997. Mechanics of single kinesin molecules measured by optical trapping nanometry. Biophys J 73:2012-22.
55. Miyata M, Ryu WS, Berg HC. 2002. Force and velocity of *Mycoplasma mobile* gliding. J Bacteriol 184:1827-31.
56. Takagi Y, Homsher EE, Goldman YE, Shuman H. 2006. Force generation in single conventional actomyosin complexes under high dynamic load. Biophys J 90:1295-307.
57. Scheffer MP, Gonzalez-Gonzalez L, Seybert A, Ratera M, Kunz M, Valpuesta JM, Fita I, Querol E, Pinol J, Martin-Benito J, Frangakis AS. 2017. Structural characterization of the NAP; the major adhesion complex of the human pathogen *Mycoplasma genitalium*. Mol Microbiol 105:869-879.
58. Nakane D, Miyata M. 2007. Cytoskeletal "Jellyfish" structure of *Mycoplasma mobile*. Proc Natl Acad Sci USA 104:19518-19523.
59. Berg HC. 2003. The rotary motor of bacterial flagella. Annu Rev Biochem 72:19-54.
60. Noji H, Ueno H, McMillan DGG. 2017. Catalytic robustness and torque generation of the F_1-ATPase. Biophys Rev 9:103-118.
61. Fraser CM, Gocayne JD, White O, Adams MD, Clayton RA, Fleischmann RD, Bult CJ, Kerlavage AR, Sutton G, Kelley JM, Fritchman RD, Weidman JF, Small KV, Sandusky M, Fuhrmann J, Nguyen D, Utterback TR, Saudek DM, Phillips CA, Merrick JM, Tomb JF, Dougherty BA, Bott KF, Hu PC, Lucier TS, Peterson SN, Smith HO, Hutchison CA, 3rd, Venter JC. 1995. The minimal gene complement of

Journal of Bacteriology

Mycoplasma genitalium. Science 270:397-403.

62. Griniuviene B, Chmieliauskaite V, Grinius L. 1974. Energy-linked transport of permeant ions in *Escherichia coli* cells: evidence for membrane potential generation by proton-pump. Biochem Biophys Res Commun 56:206-13.
63. Mates SM, Eisenberg ES, Mandel LJ, Patel L, Kaback HR, Miller MH. 1982. Membrane potential and gentamicin uptake in *Staphylococcus aureus*. Proc Natl Acad Sci U S A 79:6693-7.
64. Schiefer HG, Schummer U. 1982. The electrochemical potential across mycoplasmal membranes. Rev Infect Dis 4 Suppl:S65-70.
65. Lo CJ, Leake MC, Pilizota T, Berry RM. 2007. Nonequivalence of membrane voltage and ion-gradient as driving forces for the bacterial flagellar motor at low load. Biophys J 93:294-302.

Figures

Fig. 1 Gliding behaviors.

(A) Phase-contrast micrograph of *M. gallisepticum* cells. The cells on the glass are gliding in the direction of the membrane protrusion marked by white triangles. (B) Field image of phase-contrast micrograph (left) and cell trajectories for 30 s, changing color with time from red to blue (right). (C) Distribution of gliding speeds averaged for 60 s at 1-s intervals was fitted with a Gaussian curve (n = 231). (D) Schematic illustration showing the measurement of gliding direction (left) and the distribution of gliding directions (right). Five consecutive cell images at 5 s intervals are shown in the same field. The cell axis and gliding directions are shown by black lines and yellow sectors, respectively. The cell glided in the direction indicated by the black arrow (left). The distribution was fitted with a Gaussian curve (right). (E) Dark-field micrograph of a cell labeled with colloidal gold (left) and trajectories (right). Four consecutive images of a cell labeled with colloidal gold at 10 s intervals are shown in the same field. The cell glided in the direction indicated by the white arrow (left). The trajectories of the mass centers of the cell and colloidal gold are indicated by black and red lines, respectively (right).

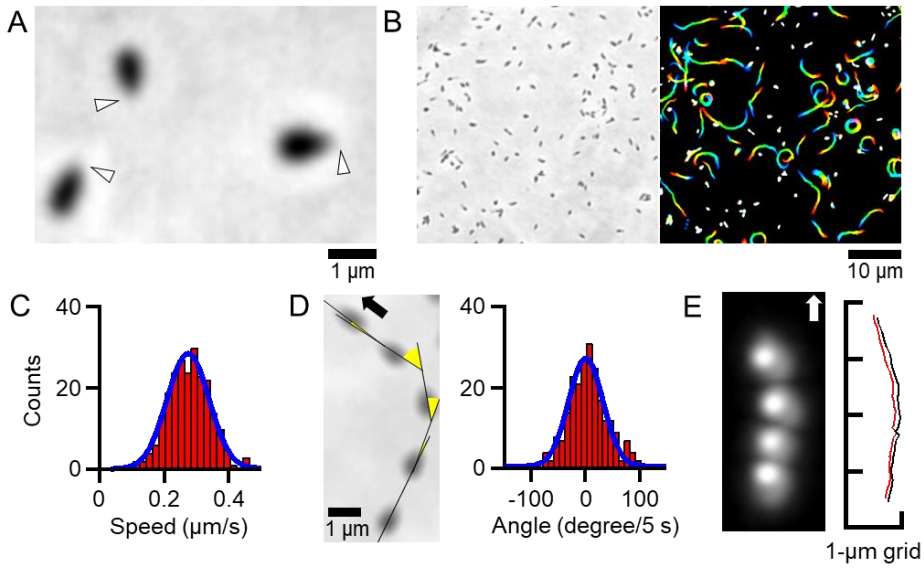

Fig. 2 Effects of MC and Ficoll on gliding.

(A) Cell trajectories for 60 s under PBS/G (top), 0.50% MC (middle) and 15% Ficoll (bottom). The color changes with time from red to blue. (B) Distributions of gliding speeds and directions under PBS/G (top), PBS/G containing 0.5% MC (middle) and 15% Ficoll (bottom) were fitted with Gaussian curves. (C) Gliding speeds and directions under various concentrations of MC or Ficoll. The average gliding speeds for 60 s at 1 s intervals and the average gliding directions every 5 s for 60 s under PBS/G containing 0%, 0.10%, 0.25%, 0.50% MC or 5%, 10%, 15% Ficoll conditions are plotted with standard deviations. Black, red, and blue circles indicate PBS/G, MC, and Ficoll, respectively.

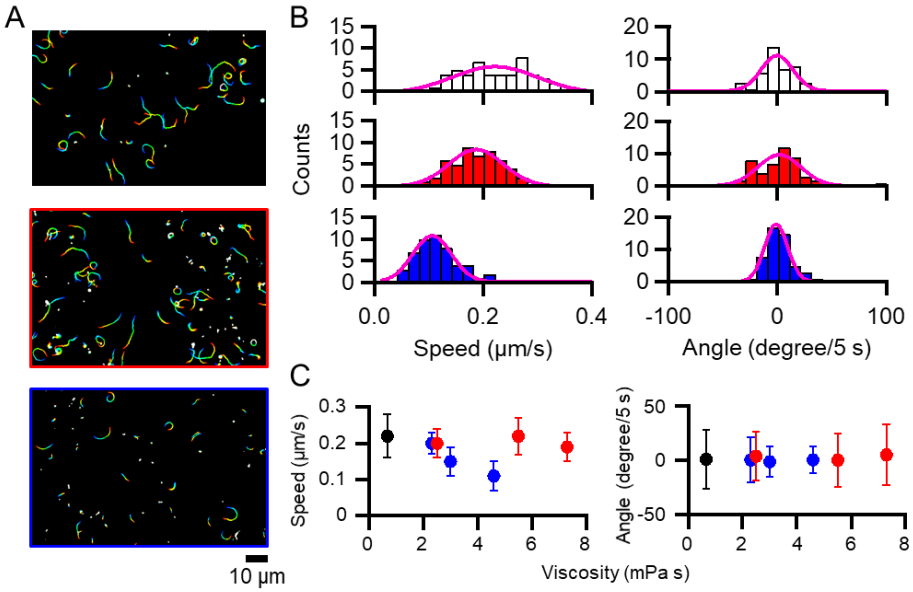

Fig. 3 Effects of SL on binding and gliding

(A) Cell trajectories for 60 s under various concentrations of SL. The color changes with time from red to blue. (B) Changes in gliding speeds by the addition of SL. Dotted lines indicate the time point when various concentrations of SL were added. The gliding speeds of individual cells are plotted as dots for every 10 s. (n_{cells} = 9, 9, 10, 6, 6, 9 for 0, 0.1, 0.2, 0.3, 0.4, 0.5 mM SL, respectively). The average gliding speeds are shown with solid lines. The gliding speeds from 0 to 10 s in each condition are normalized as 100%. (C) The gliding cell ratios under each SL concentration are plotted with standard deviations and fitted with a sigmoidal curve. (D) The gliding speeds under each SL concentration are plotted with standard deviations and fitted with a sigmoidal curve.

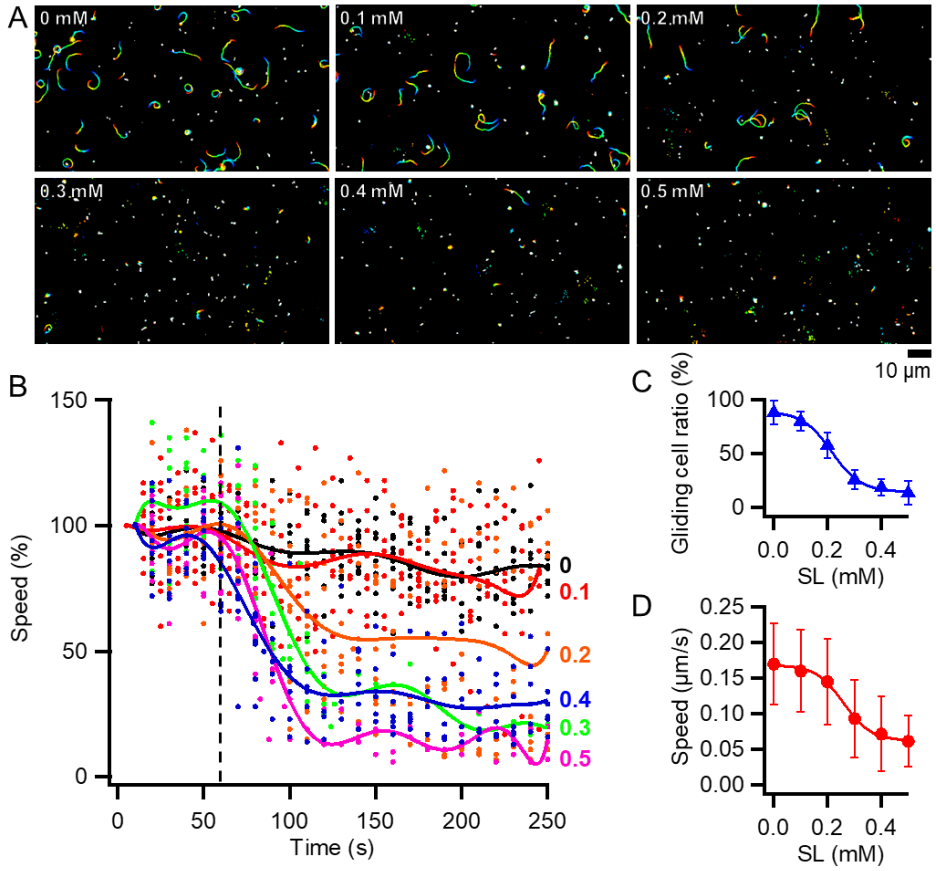

633

634

Fig. 4 Gliding ghost

(A) Trajectories for 250 s at 5 s intervals of all cells (left) and the cell to be the gliding ghost (right). The color changes with time from red to blue. The 0.007% Triton X-100 containing 1 mM ATP + 0.01 mM ADP solution was added at 0 s. (B) Phase-contrast micrographs of intact (upper), pre-permeabilized (middle) and post-permeabilized cells (lower) marked with white triangles in (A). The time points after the addition of Triton solutions are shown in each panel. (C) Transitions of gliding speeds and cell-image densities. The average gliding speeds and cell-image densities for 10 s at 1-s intervals are plotted as black circles and gray triangles, respectively. The average cell-image densities from -60 to -50 s is normalized as 100%. ‘Tri’ and ‘Per’ indicate the time points when 0.007% Triton X-100 containing 1 mM ATP + 0.01 mM ADP solution was added, and the density shift occurred, respectively. (D) The phase-contrast micrograph of cells treated with Triton solution. Cells showed three levels of cell-image density shifts; the image density did not decrease (right-upper), the image density decreased to be about 75% of the intact cell (left-upper), and the image density decreased to half of the intact cell (left-lower). (E) Distribution of cell-image densities at 90 s after the addition of Triton solution was fitted by the sum of three Gaussian curves. The individual Gaussian curves and the sum of three Gaussian curves are indicated by black broken and magenta solid lines, respectively. The cell-image density before Triton treatment is normalized as 100%. The positions of peak tops are indicated by black triangles. (F) Ghosts constructed by Triton X-100 solutions including nucleotides. Intact, pre-permeabilized, post-permeabilized, and trajectories of ghosts for 15 min are shown from left to right panels. The color changes with time from red to blue. The time points after the addition of Triton solutions are shown in each panel. The cells indicated by

black circles decrease for the cell-image densities to be about 75% at post-permeabilized panels. (G) Distribution of gliding speeds of ghosts constructed by 0.007% Triton X-100 containing 1 mM ATP + 0.01 mM ADP solution fitted with a Gaussian curve. (H) The average gliding speeds of ghosts constructed with Triton X-100 solution including ATP or ATP-V_i are shown with standard deviations. (I) The occurrence ratios of gliding ghosts to all intact cells are shown. (J) The ratios of ghosts which continued to glide through 17 min of video recording are shown.

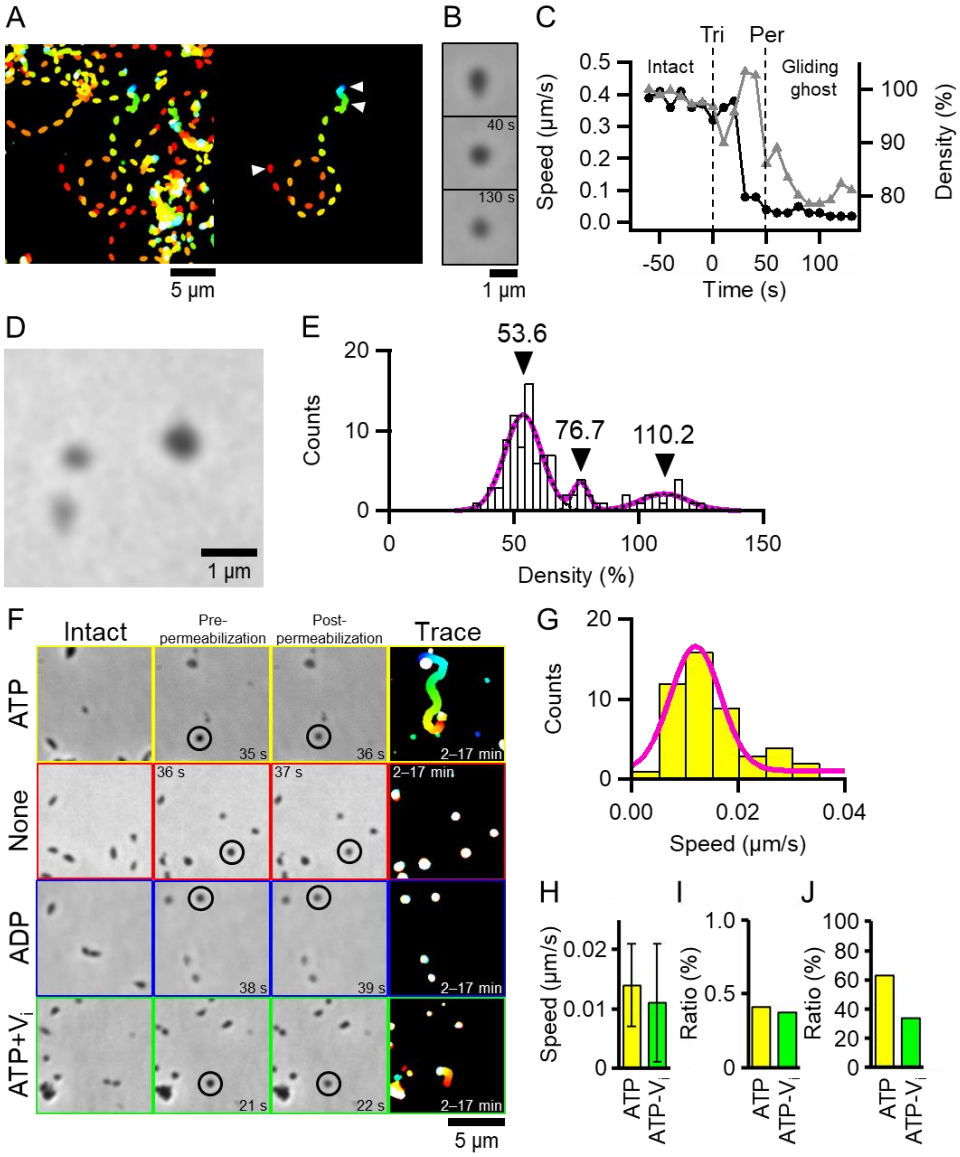

666

667

Fig. 5 Negative-staining electron micrographs of cell permeabilization.

(A) Intact cells. The cells featured by the bleb and infrableb are shown. (B–E) Cells treated with 0.007% Triton X-100 containing 1 mM ATP + 0.01 mM ADP. Some of the permeabilized cells have large (C) or small (D) holes marked by yellow triangles. (E) Magnified images of red boxed areas in (D). A–D show the same magnification. Two examples of images are shown for each category.